INORGANIC CHEMISTRY FRONTIERS

RESEARCH ARTICLE

View Article Online
View Journal | View Issue

Cite this: *Inorg. Chem. Front.*, 2020, **7**, 3379

A water-stable terbium metal–organic framework as a highly sensitive fluorescent sensor for nitrite†

Hui Min, Zongsu Han, Mengmeng Wang, Yongjie Li, Tianze Zhou, Wei Shi * and Peng Cheng *

Received 30th June 2020,
Accepted 17th July 2020

DOI: 10.1039/d0qi00780c

rsc.li/frontiers-inorganic

A novel water-stable Tb-based metal–organic framework (Tb-MOF), namely $\{[Tb(CA)(OA)_{0.5}(H_2O)_2]\cdot H_2O\}_n$ (H_2CA = chelidonic acid; H_2OA = oxalic acid), was synthesized *via* a solvothermal method. Tb-MOF was studied for its highly sensitive detection towards nitrite, which is a hazardous chemical in water and food. As a luminescent sensor, Tb-MOF displays a linear detection range between 0 and 15.6 μM, with a limit of detection of 28.25 nM. Dynamic quenching process was observed in this system and was studied in detail. A mechanism study revealed that the fluorescence response of Tb-MOF towards nitrite was due to the energy transfer from the sensitized Tb^{3+} ion to the nitrite.

1. Introduction

Recently, metal–organic frameworks (MOFs) have evoked intensive interests owing to their intrinsic features such as varied structures, permanent porosity and adjustable functionality.[1–3] Inclusive applications in gas adsorption and separation,[4,5] catalysis,[6,7] sensors,[8–11] magnetic materials,[12] drug release[13,14] and energy-related areas[15–17] have been explored. For the MOFs with sensing-based applications,[18–20] lanthanide MOFs (Ln-MOFs) have displayed excellent luminescence properties that can be taken into consideration.[21,22] Through the reasonable adjustment of the host–guest interactions, Ln-MOFs have been applied in the chemical sensing of ions,[23–25] organic small molecules,[26,27] volatile organic compounds (VOCs)[28] and gases,[29–31] nitro explosives,[32–34] biomolecules[35,36] and so on.

Nitrite (NO_2^-) ion is widely used in pickled products but it has a great potential threat to human health because of the generation of carcinogenic *N*-nitrosamines *in vivo* from the ingested nitrite.[37] Medical issues such as oesophageal cancer and birth defects have been reported due to the excessive consumption of nitrite ions.[38] According to the World Health Organization guidelines, the maximum contaminant level (MCL) of nitrite ions in drinking water is 3 mg L^{-1} (65 μM).[39] Traditional nitrite ion detection was performed using toxic naphthyl ethylenediamine *via* colorimetry assay.[40] To avoid the usage of toxic materials, other methods including chromatography,[41] electrochemical techniques[42] and fluorescent technology[43–45] have been developed. However, these methods need complicated instruments, tedious detection procedures, and are time-consuming. Among these methods, the fluorescence sensing technology include the advantages of rapid response, low cost and easy-operation.[46]

In this study, based on the fluorescence sensing mechanism and our experience on MOF-based sensing materials,[47–56] a new water-stable Tb-based MOF (Tb-MOF), $\{[Tb(CA)(OA)_{0.5}(H_2O)_2]\cdot H_2O\}_n$ (H_2CA = chelidonic acid; H_2OA = oxalic acid) was synthesized for highly sensitive nitrite detection. An isomorphic Gd-MOF was also synthesized for the mechanism studies. The dynamic quenching mechanism of Tb-MOF with nitrite provides a large quenching rate constant (k_q) of 1.16×10^9 M^{-1} s^{-1}. Both the high k_q and the low limit of detection (LOD) of 28.25 nM indicate a high sensitivity of Tb-MOF towards nitrite ion.

2. Experimental

2.1 Materials and methods

All purchased chemicals were of reagent grade and were used directly. Fourier transform infrared (FT-IR) spectra were carried out on a Bruker ALPHA spectrophotometer. Elemental analyses (EA) for C and H were executed on a PerkinElmer 240 CHN elemental analyzer. Ultraviolet visible (UV–vis) spectra were acquired using a Shimadzu UV-2600 spectrophotometer. Powder X-ray diffraction (PXRD) patterns were recorded on a Rigaku Smartlab SE X-ray diffractometer. Thermogravimetric analysis (TGA) was performed on a Labsys NETZSCH TG209

Key Laboratory of Advanced Energy Materials Chemistry (MOE), College of Chemistry, Nankai University, Tianjin, 300071, China.
E-mail: shiwei@nankai.edu.cn, pcheng@nankai.edu.cn

†Electronic supplementary information (ESI) available: Crystallographic data of Tb-MOF, PXRD, TGA and other figures and tables. CCDC 2011050. For ESI and crystallographic data in CIF or other electronic format see DOI: 10.1039/d0qi00780c

Setaram apparatus in nitrogen atmosphere (at the heating rate of 10 °C min^{-1}). Luminescence-related spectra were recorded on a FS-5 fluorescence spectrophotometer.

2.2 Synthesis

The synthesis of $\{[Tb(CA)(OA)_{0.5}(H_2O)_2]\cdot H_2O\}_n$: Terbium nitrate hexahydrate (0.0453 g, 0.1 mmol), chelidonic acid (0.0272 g, 0.15 mmol) and CH_3CN/H_2O (v : v = 3 : 1; 8 mL in total) were successively placed in a 25 mL Teflon-lined stainless steel reactor. The reactor was heated at 95 °C for three days with an additional one day cooling to 30 °C. Light yellow crystals were selected and washed with water and acetonitrile with 28.9% yield based on terbium nitrate hexahydrate. EA calculated: C, 21.01%; H, 2.19%. Found: C, 21.42%; H, 2.12%. IR data (cm^{-1}): 3603 (s), 3175 (br), 1717 (s), 1618 (d), 1363 (t), 1212 (s), 1122 (s), 925 (d), 792 (s), 716 (s), 537 (m), 442(s).

Gd-MOF was obtained *via* the same method used for Tb-MOF by replacing terbium nitrate with gadolinium nitrate.

2.3 X-ray crystallography

Using an Agilent Technologies SuperNova single-crystal diffractometer equipped with graphite-monochromatic Mo-Kα radiation (λ = 0.71073 Å), the crystal data of Tb-MOF was collected at 120 K. The structure was solved by SHELXS (direct methods) and refined by SHELXL (full matrix least-squares techniques) in the Olex2 package.[57,58] The parameters, data collection, and refinements of the single crystal are summarized in Table S1.† CCDC 2011050† contains the details of the crystal structure.

2.4 Luminescence measurements

Tb-MOF (30 mg) was finely ground. This powder was then scattered in distilled water (100 mL). An aqueous suspension of Tb-MOF was obtained after ultrasonicating it for 10 min. After the suspension was stabilized, luminescence tests were performed using 3 mL of supernatant. The luminescence spectra of Tb-MOF suspension were measured *in situ* with freshly prepared 0.4 mM analyte solutions.

3. Results and discussion

3.1 Structural description and characterizations

Crystallized in the $P\bar{1}$ space group, the asymmetric unit of Tb-MOF contains one Tb^{3+} ion, two coordinated water molecules, one solvent water molecule, one CA^{2-} ligand and a half OA^{2-} ligand. Eight oxygen atoms coordinate to the Tb^{3+} ion, completing a triangular dodecahedron configuration (Fig. 1a and b). Four oxygen atoms are from two CA^{2-}, including three carboxylate oxygen atoms (Tb–O bond lengths ranging from 2.304(10) Å to 2.428(10) Å) and a carbonyl oxygen atom (the bond length of Tb–O is 2.366(9) Å). Two oxygen atoms are from two coordinated water molecules (Tb–O bond lengths of 2.380(10) Å and 2.407(10) Å). Rest of the two oxygen atoms are from the carboxylate oxygen atoms of the oxalates derived from the partial decomposition of H_2CA (Tb–O bond lengths of 2.399(9) Å and 2.402(9) Å). Tb^{3+} ions are connected by CA^{2-} ions in chains (Fig. 1c) and these chains are connected into a layer by CA^{2-} (Fig. 1d). The layers are further connected by OA^{2-} into a three-dimensional framework (Fig. 1e). Taking OA^{2-}, CA^{2-} and Tb^{3+} ions as two, four and five-connected nodes, respectively, the framework is simplified as a (2,4,5)-connected trinodal net with a short (Schläfli) vertex symbol of $\{4^4\cdot6^2\cdot8^4\}^2\{4^4\cdot6^2\}^2\{8\}$ (Fig. S1†).

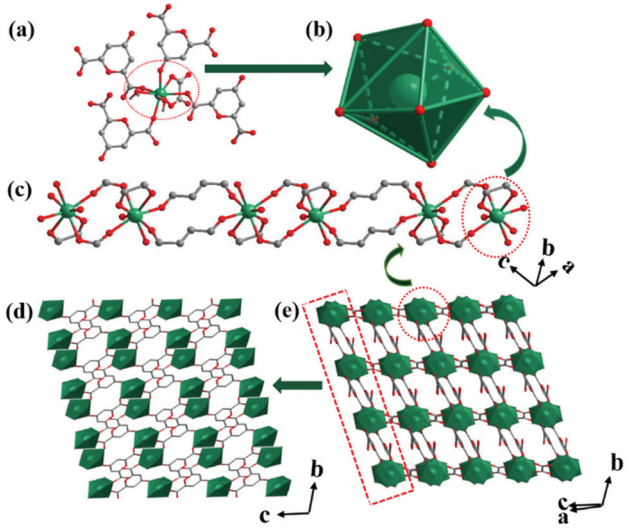

Fig. 1 Coordination environment (a) and coordination geometry (b) of Tb^{3+} ion; (c) the connection mode of TbO_8; (d) 2D layer of Tb-MOF along the *a* axis; (e) 3D framework of Tb-MOF. Atom codes: Tb (green), O (red), C (gray). Hydrogen atoms are removed for clarity.

PXRD showed that the diffraction peaks of the as-synthesized Tb-MOF are accorded with the calculated ones from the crystal data (Fig. S2†). This result confirms the high phase purity of the as-synthesized Tb-MOF. In addition, the diffraction peaks of Tb-MOF after immersion in water for 36 h agree well with that of the primitive data. The results also indicate the high water-stability of Tb-MOF, which benefits from the suitable coordination models and rigid framework of Tb-MOF. The TGA of Tb-MOF displays a weight loss of 11.96% below 195 °C, which corresponds to the release of three water molecules (Fig. S3,† calc. 11.81%). Further heating causes a dramatic weight loss, indicating the disintegration of Tb-MOF.

3.2 Luminescence study and detection of nitrite

The luminescence spectrum is shown in Fig. 2. The excitation spectrum was recorded at a wavelength of 544 nm, which exhibited a broad band with a peak at 295 nm. Excited by 295 nm ultraviolet light, Tb-MOF displayed four well-resolved characteristic emissions at 489, 545, 585 and 621 nm, corresponding to the $^5D_4 \rightarrow {}^7F_J$ (J = 6, 5, 4, and 3) transitions of Tb^{3+} ions, respectively. The schematic energy transfer process within Tb-MOF is shown in Fig. S4.† The singlet and triplet levels of the ligands were calculated through the UV-Vis spectrum (Fig. S5a†) and phosphorescence spectrum of the isomorphic Gd-MOF at 77 K (Fig. S5b†). The singlet level of H_2OA is observed at 39 582 cm^{-1} (252 nm), in accordance with our

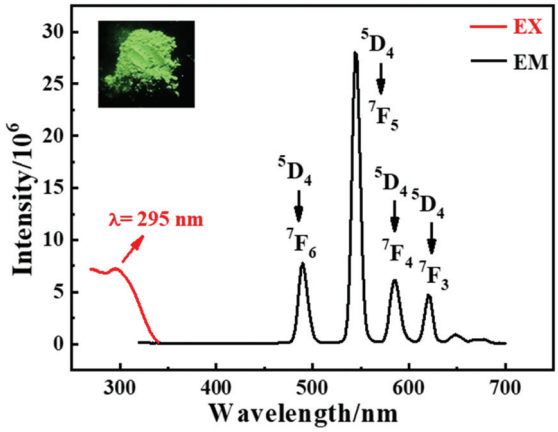

Fig. 2 The luminescence spectra of Tb-MOF. The inset picture is Tb-MOF excited under a 254 nm ultraviolet lamp.

previous study,[52] while the singlet level of H_2CA is at 33 630 cm^{-1} (273 nm). The triplet levels of OA^{2-} and CA^{2-} are 24 390 cm^{-1} (410 nm) and 22 831 cm^{-1} (438 nm), respectively. The energy gaps (ΔE) between the singlet-state and triplet-state energy levels of the ligands are 12 647 cm^{-1} and 10 799 cm^{-1}, respectively. The values of ΔE are much higher than 5000 cm^{-1}, indicating effective intersystem crossing processes using the Reinhold's empirical rule.[59,60] Hence, the gaps of the triplet level of the ligands and the $^5D_4$ energy level of the Tb^{3+} ion (20 500 cm^{-1}) are 3890 cm^{-1} (H_2OA) and 2331 cm^{-1} (H_2CA) in the range of the most capable values (2500–4500 cm^{-1}),[61] which indicates an effective energy transfer process from CA^{2-}/OA^{2-} to Tb^{3+} ion, giving rise to a bright green emission when exposed to 254 nm UV light (Fig. 2, inset).

For studying the selectivity of Tb-MOF in water, the quenching effects of different salts were studied. The luminescence intensities of Tb-MOF with other salts have almost no change except that with the nitrite salt (Fig. 3a). A certain degree of fluorescence quenching of Tb-MOF occurs in the presence of Fe^{3+}, Cu^{2+} and PO_4^{3-}. However, when nitrite was added, a clear quenching effect occurred, indicating selectivity of Tb-MOF towards nitrite ions. The quenching efficiencies were calculated by $(I_0 - I)/I_0$, as shown in Fig. 3b, where I_0 and I are intensities at 544 nm of Tb-MOF dispersions without or with the addition of different salts, respectively. In particular, nitrite ions exhibited a quenching efficiency of 82.3%. Compared with Fe^{3+}, Cu^{2+} and PO_4^{3-}, the much higher quenching efficiency of $NaNO_2$ indicated the excellent selectivity of Tb-MOF towards nitrite ions. The results indicated that Tb-MOF can be used for the specific detection of nitrite.

To improve the accuracy for the detection of nitrite ions, three different fluorescence titration experiments were performed by adding different volumes of nitrite ions (3 μL, 5 μL, and 10 μL). Considering the first one for example, the luminescence intensities of Tb-MOF with successive additions of 3 μL nitrite are shown in Fig. S6.† The fluorescence quenching

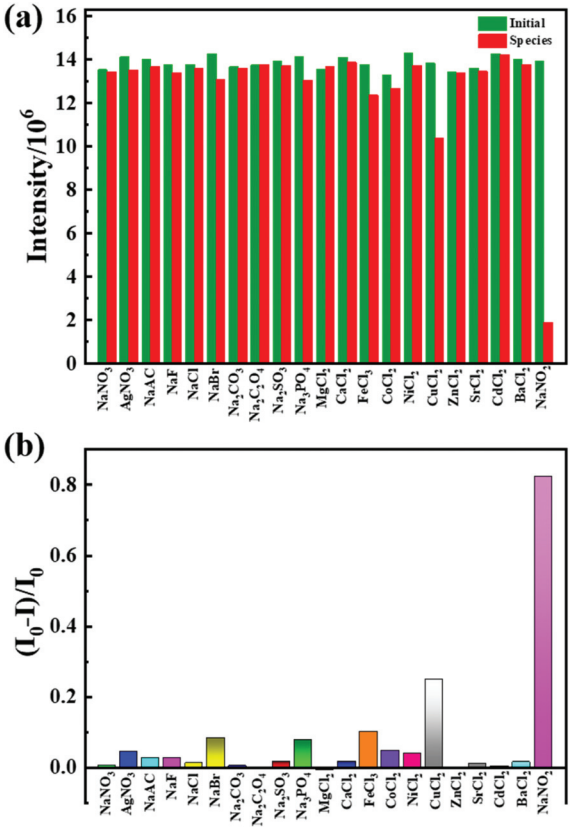

Fig. 3 (a) Fluorescence intensities of Tb-MOF without or with different species. (b) the quenching efficiency of different salts.

result of Tb-MOF is quantitatively mustered using the Stern–Volmer (S–V) eqn (1):

$$I_0/I = 1 + K_{SV}[C] \quad (1)$$

where K_{SV} is the S–V quenching constant (M^{-1}), $[C]$ is the nitrite ion concentration, and I_0 and I are fluorescence intensities without and with adding nitrite ions in dispersions, respectively. In Fig. S7,† the linear equation is well fitted with $I_0/I - 1 = 0.474[C] + 0.016$ in the range of 0–6 μM with a R^2 of 0.999. The K_{SV} value of Tb-MOF is 4.74×10^5 M^{-1}. The K_{SV} value is higher than that of most MOF-based ion sensing materials (usually 10^3–10^4 M^{-1}), indicating a high sensitivity of Tb-MOF towards nitrite.[23–25] The results of the three sets of fluorescence titrations (Fig. S6–S11†) were combined in Fig. 4. The linear correlation was further modified as $I_0/I - 1 = 0.482[C] + 0.002$ with a R^2 of 0.999 in the range of 0–15.6 μM, with the K_{SV} value of 4.82×10^5 M^{-1}.

The LOD was calculated using the 3σ IUPAC criteria by eqn (2) and (3):

$$S_d = \sqrt{\frac{1}{N-1}\sum_{i=1}^{N}(I_0/I_i - I_{av})^2 (i = 1, 2, 3, \ldots N)} \quad (2)$$

$$\mathrm{LOD} = 3S_d/\mathrm{slope} \quad (3)$$

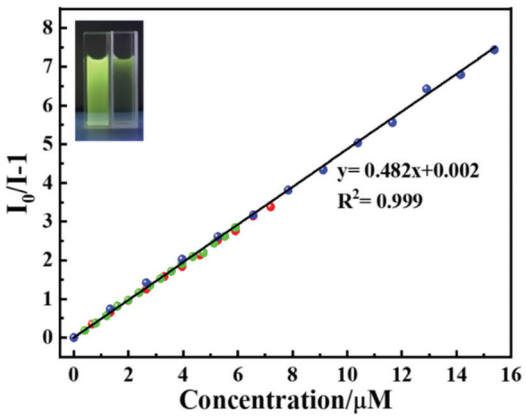

Fig. 4 Summary of S–V plots at 544 nm of Tb-MOF towards nitrite ions with different volumes, 3 μL (green plots), 5 μL (red plots), 10 μL (blue plots). Inset is the picture of Tb-MOF suspension excited by 254 nm ultraviolet light before and after adding 20 μL nitrite aqueous solution (4 mM).

where S_d is the standard deviation of the replicate fluorescence intensities of Tb-MOF dispersions performed twenty times (Fig. S12†). I_i is the fluorescence intensity at 544 nm without nitrite, and I_{av} is the average of I_0/I_i. The slope value was calculated from eqn (1) and the LOD was calculated to be 28.25 nM, which is far below the criterion of the World Health Organization for drinking water.

To investigate the practical application, Tb-MOF was employed to measure the nitrite concentration in tap water. The related results of spike-and-recovery experiences are shown in Table S2.† The recoveries were found to be 97.7–100.9%. Moreover, the anti-interference of Tb-MOF was also evaluated (Fig. S13†). With coexisting anions and cations, the degree of the quenched fluorescence of Tb-MOF stayed almost the same after the addition of nitrite, indicating that Tb-MOF displayed a considerable anti-interference ability. The recycling performance of Tb-MOF was also studied (Fig. 5). The suspensions with nitrite ions were centrifuged and washed with water and acetonitrile for several times after the sensing experiments. It was found that the luminescence intensity can be recycled at least 5 times. All these results indicate that Tb-MOF has potential applications in the nitrite ion detection in polluted water and food preservatives.

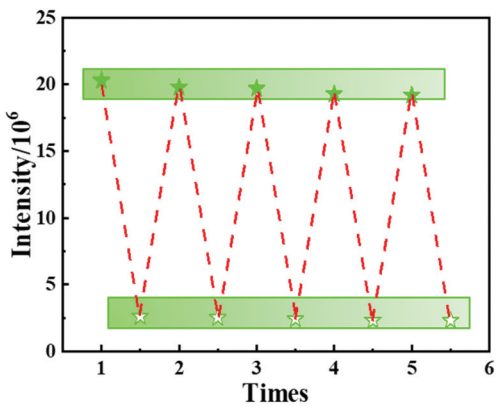

Fig. 5 Reproducibility of Tb-MOF with five continuous quenching cycles.

3.3 Sensing mechanism

To the best of our knowledge, this sensing material provides the lowest LOD (28.25 nM) for the nitrite ion detection amongst the reported MOF-based fluorescence sensing materials (Table S3†). To figure out the quenching behaviour towards nitrite ions, the sensing mechanism was investigated. First, the PXRD of Tb-MOF immersed in 4 mM nitrite ions for 4 h showed similar results to that obtained with the calculated data (Fig. S14†), indicating the structural stability of Tb-MOF with nitrite ions. As shown in Fig. 4, the S–V plots show a linear relationship at the completed concentration range, which is different from that of the concentration controlled by a self-absorption process.[51–55] The luminescence lifetimes of Tb-MOF were measured at 544 nm with different concentrations of the nitrite ions (Fig. S15 and Table S4†). The lifetimes decrease with the increase in the concentration of nitrite ions, and the lifetime-based S–V curve provides a same K_{SV} of 4.82×10^5 M^{-1} (Fig. S16†) with that of the S–V curve, indicating a dynamic quenching progress. The quenching rate constant (k_q) can be calculated using eqn (4):

$$k_q = K_{SV}/\tau_0 \quad (4)$$

where K_{SV} is lifetime-based S–V quenching constant (M^{-1}), and τ_0 is the luminescence lifetime (s^{-1}) of Tb-MOF without nitrite ions. The k_q value was 1.16×10^9 M^{-1} s^{-1}, which is 10 times lower than that of the purely diffusion-controlled quenching process (about 10^{10} M^{-1} s^{-1})[62] possibly due to the steric hindrance of Tb-MOF, limiting the number of collisional quenching occurring.[23,63] The decrease in lifetimes indicates the presence of other relaxation pathway that can depopulate the excited state. To further understand the specific energy transfer between Tb-MOF and nitrite ions, the singlet and triplet energy levels of $NaNO_2$ were obtained as 48 077 cm^{-1} (208 nm) and 19 084 cm^{-1} (524 nm) (Fig. S17 and S18†), which are similar to the results reported by Fujio.[64,65] The triplet level of $NaNO_2$ is slightly lower than the $^5D_4$ energy level of the Tb^{3+} ion (20 500 cm^{-1}) with a gap of 1416 cm^{-1}, which is lower than 1850 cm^{-1}. This result indicates that energy transfer between Tb-MOF and $NaNO_2$ is possible.[61,66] In addition, no obvious overlap was observed between the UV-Vis spectra of the ligands and $NaNO_2$ (Fig. S5a and S17†), which excludes the possibility of the competitive absorption mechanism.

Based on the above analysis, the mechanism of the sensing function is shown in Fig. 6. Excited at 295 nm, the Tb^{3+} ion is sensitized by antenna effect and displays characteristic emissions; when nitrite ion was added, dynamic quenching behaviour between Tb-MOF and nitrite ion happened. In this process, energy transfer between Tb-MOF and nitrite ion occurred, leading to the decrease in the emission intensity.

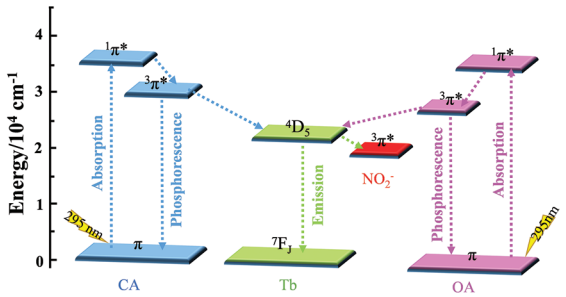

Fig. 6 The schematic energy transfer process of Tb-MOF in the presence of nitrite.

4. Conclusions

In summary, a water-stable Tb-based MOF was synthesized as a sensitive and selective nitrite ion sensor. The sensing mechanism studies show that in the presence of nitrite ions, a part of the energy for the emission of Tb-MOF is transferred to nitrite ion, hence decreasing the emission intensity. To the best of our knowledge, the sensor provides the lowest LOD (28.25 nM) for the nitrite ion detection compared with the recently reported MOF-based fluorescence sensing materials for nitrite. The satisfactory recyclability, sensitivity, selectivity, and stability indicate a promising utilization of Tb-MOF for nitrite detection in water.

Conflicts of interest

There are no conflicts to declare.

Acknowledgements

This work was supported by the National Natural Science Foundation of China (grant numbers 21931004 and 21861130354), the Natural Science Foundation of Tianjin (18JCJQJC47200), the Fundamental Research Funds for the Central Universities, Nankai University (63201016 and 63201043) and the Ministry of Education of China (grant number B12015). W. S. acknowledges the receipt of a Newton Advanced Fellowship from Royal Society.

References

1 O. M. Yaghi, M. J. Kalmutzki and C. S. Diercks, *Introduction to Reticular Chemistry, Metal-Organic Framework and Covalent Organic Frameworks*, 2019, WILEY-VCH.
2 G. Maurin, C. Serre, A. Cooper and G. Férey, The new age of MOFs and of their porous-related solids, *Chem. Soc. Rev.*, 2017, **46**, 3104.
3 B. Li, H. Wen, Y. Cui, W. Zhou, G. Qian and B. Chen, Emerging Multifunctional Metal-Organic Framework Materials, *Adv. Mater.*, 2016, **28**, 8819.
4 D. Xue, Q. Wang and J. Bai, Amide-functionalized metal–organic frameworks: Syntheses, structures and improved gas storage and separation properties, *Coord. Chem. Rev.*, 2017, **378**, 2.
5 M. S. Derry, Jr., J. C. Moreton, L. Benz and S. M. Cohen, Metal–organic frameworks for membrane-based separations, *Nat. Rev. Mater.*, 2016, **1**, 16078.
6 R. Zhang, B. Wu, Q. Li, L. Lu, W. Shi and P. Cheng, Design strategies and mechanism studies of CO_2 electroreduction catalyst based on coordination chemistry, *Coord. Chem. Rev.*, 2020, **422**, DOI: 10.1016/j.ccr.2020.213436.
7 L. Chen and Q. Xu, Metal-Organic Framework Composites for Catalysis, *Matter*, 2019, **1**, 57.
8 J. Liu, Z. Luo, Y. Pan, A. K. Singh, M. Trivedi and A. Kumar, Recent developments in luminescent coordination polymers: Designing strategies, sensing application and theoretical evidences, *Coord. Chem. Rev.*, 2020, **406**, 213145.
9 S.-Y. Zhang, Z.-Y. Wang, J. Gao, K. Wang, E. Gianolio, S. Aime, W. Shi, P. Cheng and M. J. Zaworotko, A Gadolinium(III) Zeolite-like Metal-Organic Framework-based Magnetic Resonance Thermometer, *Chem*, 2019, **5**, 1609.
10 Y. Cui, J. Zhang, H. He and G. Qian, Photonic functional metal-organic frameworks, *Chem. Soc. Rev.*, 2018, **47**, 5740.
11 F. Yi, D. Chen, M. Wu, L. Han and H. Jiang, Chemical Sensors Based on Metal–Organic Frameworks, *ChemPlusChem*, 2016, **81**, 675.
12 K. Liu, X. Zhang, X. Meng, W. Shi, P. Cheng and A. K. Powell, Constraining the coordination geometries of lanthanide centers and magnetic building blocks in frameworks: a new strategy for molecular nanomagnets, *Chem. Soc. Rev.*, 2016, **45**, 2423.
13 W. Cai, J. Wang, C. Chu, W. Chen, C. Wu and G. Liu, Metal Organic Framework-Based Stimuli-Responsive Systems for Drug Delivery, *Adv. Sci.*, 2019, **6**, 1801526.
14 M. Giménez-Marqués, T. Hidalgo, C. Serre and P. Horcajada, Nanostructured metal–organic frameworks and their bio-related applications, *Coord. Chem. Rev.*, 2016, **307**, 342.
15 L. Jiao and H. Jiang, Metal-Organic-Framework-Based Single-Atom Catalysts for Energy Applications, *Chem*, 2019, **5**, 786.
16 J. W. Liu, D. X. Xie, W. Shi and P. Cheng, Coordination compounds in lithium storage and lithium-ion transport, *Chem. Soc. Rev.*, 2020, **49**, 1624.
17 Y. Wang, Q. Li, W. Shi and P. Cheng, The application of metal-organic frameworks in electrocatalytic nitrogen reduction, *Chin. Chem. Lett.*, 2020, **31**, 1768.
18 W. P. Lustig and J. Li, Luminescent metal–organic frameworks and coordination polymers as alternative phosphors for energy efficient lighting devices, *Coord. Chem. Rev.*, 2018, **373**, 116.
19 J. Hao, X. Xu, H. Fei, L. Li and B. Yan, Functionalization of Metal–Organic Frameworks for Photoactive Materials, *Adv. Mater.*, 2018, **30**, 1705634.

20 W. P. Lustig, S. Mukherjee, N. D. Rudd, A. V. Desai, J. Li and S. K. Ghosh, Metal–organic frameworks: functional luminescent and photonic materials for sensing applications, *Chem. Soc. Rev.*, 2017, **46**, 3242.
21 P. Cheng, *Lanthanide Metal-Organic Frameworks*, Springer, 2015.
22 S. Zhao, G. Wang, D. Poelman and P. V. D. Voort, Luminescent Lanthanide MOFs: A Unique Platform for Chemical Sensing, *Materials*, 2018, **11**, 572.
23 F. M. Ebrahim, T. N. Nguyen, S. Shyshkanov, A. Gładysiak, P. Favre, A. Zacharia, G. Itskos, P. J. Dyson and K. C. Stylianou, Selective, Fast-Response, and Regenerable Metal–Organic Framework for Sampling Excess Fluoride Levels in Drinking Water, *J. Am. Chem. Soc.*, 2019, **141**, 3052.
24 H. Chen, P. Fan, X. Tu, H. Min, X. Yu, X. Li, J. L. Zeng, S. Zhang and P. Cheng, A Bifunctional Luminescent Metal–Organic Framework for the Sensing of Paraquat and Fe^{3+} Ions in Water, *Chem. – Asian J.*, 2019, **14**, 3611.
25 Z. Yang, M. Wang, X. Wang and X. Yin, Boric-Acid-Functional Lanthanide Metal–Organic Frameworks for Selective Ratiometric Fluorescence Detection of Fluoride Ions, *Anal. Chem.*, 2017, **89**, 1930.
26 T. Song, K. Yuan, W. Qian, Y. Shi, J. Dong, H. Gao, X. Yang, J. Cui and B. Zhao, Water Stable [Tb_4] Cluster-Based Metal–Organic Framework as Sensitive and Recyclable Luminescence Sensor of Quercetin, *Anal. Chem.*, 2019, **91**(4), 2595.
27 Y. Gao, G. Yu, K. Liu and B. Wang, Luminescent mixed-crystal Ln-MOF thin film for the recognition and detection of pharmaceuticals, *Sens. Actuators, B*, 2018, **257**, 931.
28 H. Zhao, J. Ni, J. Zhang, S. Liu, Y. Sun, H. Zhou, Y. Li and C. Duan, A trichromatic MOF composite for multidimensional ratiometric luminescent sensing, *Chem. Sci.*, 2018, **9**, 2918.
29 J. Peng, C. L. Teoh, X. Zeng, A. Samanta, L. Wang, W. Xu, D. Su, L. Yuan, X. Liu and Y. Chang, Development of a highly selective, sensitive, and fast response upconversion luminescent platform for hydrogen sulfide detection, *Adv. Funct. Mater.*, 2016, **26**, 191.
30 C. Wang, L. Li, J. G. Bell, X. Lv, S. Tang, X. Zhao and K. M. Thomas, Hysteretic gas and vapor sorption in flexible interpenetrated lanthanide-based metal-organic frameworks with coordinated molecular gating via reversible single-crystal-to-single-crystal transformation for enhanced selectivity, *Chem. Mater.*, 2015, **27**, 1502.
31 J. Hao and B. Yan, A dual-emitting 4d-4f nanocrystalline metal-organic framework as a self-calibrating luminescent sensor for indoor formaldehyde pollution, *Nanoscale*, 2016, **8**, 12047.
32 X. Z. Song, S. Y. Song, S. N. Zhao, Z. M. Hao, M. Zhu, X. Meng, L. L. Wu and H. J. Zhang, Single-crystal-to-single-crystal transformation of a europium(III) metal-organic framework producing a multi-responsive luminescent sensor, *Adv. Funct. Mater.*, 2014, **24**, 4034.
33 W. Xie, S. R. Zhang, D. Y. Du, J. S. Qin, S. J. Bao, J. Li, Z. M. Su, W. W. He, Q. Fu and Y. Q. Lan, Stable luminescent metal-organic frameworks as dual-functional materials to encapsulate Ln^{3+} ions for white-light emission and to detect nitroaromatic explosives, *Inorg. Chem.*, 2015, **54**, 3290.
34 B. Wang, X. L. Lv, D. W. Feng, L. H. Xie, J. Zhang, M. Li, Y. B. Xie, J. R. Li and H. C. Zhou, Highly stable Zr(IV)-based metal-organic frameworks for the detection and removal of antibiotics and organic explosives in water, *J. Am. Chem. Soc.*, 2016, **138**, 6204.
35 J. Hao and B. Yan, Determination of urinary 1-hydroxypyrene for biomonitoring of human exposure to polycyclic aromatic hydrocarbons carcinogens by a lanthanide-functionalized metal-organic framework sensor, *Adv. Funct. Mater.*, 2017, **27**, 1603856.
36 T. Xia, Y. Wan, Y. Li and J. Zhang, Highly Stable Lanthanide Metal–Organic Framework as an Internal Calibrated Luminescent Sensor for Glutamic Acid, a Neuropathy Biomarker, *Inorg. Chem.*, 2020, **59**, 8809.
37 A. J. Cross, L. M. Ferrucci, A. Risch, B. I. Graubard, M. H. Ward, Y. Park, A. R. Hollenbeck, A. Schatzkin and R. Sinha, A Large Prospective Study of Meat Consumption and Colorectal Cancer Risk: An Investigation of Potential Mechanisms Underlying this Association, *Cancer Res.*, 2010, **70**, 2406.
38 L. B. Maia and J. J. G. Moura, How Biology Handles Nitrite, *Chem. Rev.*, 2014, **114**, 5273.
39 World Health Organization, *Guidelines for Drinking Water Quality*, WHO Press, Geneva, Switzerland, 3rd edn, 2008.
40 T. L. Mako, A. M. Levenson and M. Levine, Ultrasensitive Detection of Nitrite through Implementation of N-(1-Naphthyl)ethylenediamine-Grafted Cellulose into a Paper-Based Device, *ACS Sens.*, 2020, **5**, 1207.
41 C. Lopez-Moreno, I. V. Perez and A. M. Urbano, Development and validation of an ionic chromatography method for the determination of nitrate, nitrite and chloride in meat, *Food Chem.*, 2016, **194**, 687.
42 H. Chen, T. Yang, F. Liu and W. Li, Electrodeposition of gold nanoparticles on Cu-based metal-organic framework for the electrochemical detection of nitrite, *Sens. Actuators, B*, 2019, **286**, 401.
43 Y. Zhan, Y. Zeng, L. Li, F. Luo, B. Qiu, Z. Lin and L. Guo, Ratiometric Fluorescent Hydrogel Test Kit for On-Spot Visual Detection of Nitrite, *ACS Sens.*, 2019, **4**, 1252.
44 Su Zhu, L. Zhao and B. Yan, A novel spectroscopic probe for detecting food preservative NO_2^-: Citric acid functionalized metal-organic framework and luminescence sensing, *Microchem. J.*, 2020, **155**, 104768.
45 J. Wu and B. Yan, Luminescent Hybrid Tb^{3+} Functionalized Metal–Organic Frameworks Act as Food Preservative Sensor and Water Scavenger for NO_2^-, *Ind. Eng. Chem. Res.*, 2018, **57**, 7105.
46 Z. Hu, B. J. Deibert and J. Li, Luminescent metal–organic frameworks for chemical sensing and explosive detection, *Chem. Soc. Rev.*, 2014, **43**, 5815.
47 S. Wu, H. Min, W. Shi and P. Cheng, Multicenter Metal-Organic Framework-Based Ratiometric Fluorescent Sensors, *Adv. Mater.*, 2020, **32**, 1805871.

48 Y. Lin, X. Zhang, W. Chen, W. Shi and P. Cheng, Three Cadmium Coordination Polymers with Carboxylate and Pyridine Mixed Ligands: Luminescent Sensors for Fe^{III} and Cr^{VI} Ions in an Aqueous Medium, *Inorg. Chem.*, 2017, **56**, 11768.

49 J. Zhou, H. Li, H. Zhang, H. Li, W. Shi and P. Cheng, A bimetallic lanthanide metal-organic material as a selfcalibrating color-gradient luminescent sensor, *Adv. Mater.*, 2015, **27**, 7072.

50 Z. Han, K. Wang, Y. Guo, W. Chen, J. Zhang, X. Zhang, G. Siligardi, S. Yang, Z. Zhou, P. Sun, W. Shi and P. Cheng, Cation-induced chirality in a bifunctional metalorganic framework for quantitative enantioselective recognition, *Nat. Commun.*, 2019, **10**, 5117.

51 S. Zhang, W. Shi, P. Cheng and M. J. Zaworotko, A Mixed-Crystal Lanthanide Zeolite-like Metal–Organic Framework as a Fluorescent Indicator for Lysophosphatidic Acid, a Cancer Biomarker, *J. Am. Chem. Soc.*, 2015, **137**, 12203.

52 H. Ma, L. Wang, J. Chen, X. Zhang, L. Wang, N. Xu, G. Yang and P. Cheng, A multi-responsive luminescent sensor for organic small-molecule pollutants and metal ions based on a 4d–4f metal–organic framework, *Dalton Trans.*, 2017, **46**, 3526.

53 H. Zhang, D. M. Chen, H. L. Ma and P. Cheng, Real-time detection of traces of benzaldehyde in benzyl alcohol as a solvent by a flexible lanthanide microporous metal-organic framework, *Chem. – Eur. J.*, 2015, **21**, 15854.

54 Q. Xu, Z. Chen, H. Min, F. Song, Y. Wang, W. Shi and P. Cheng, Water Stable Heterometallic Zn-Tb Coordination Polymer for Rapid Detection of the Ultraviolet Filter Benzophenone, *Inorg. Chem.*, 2020, **59**, 6729.

55 S. Wu, Y. Lin, J. Liu, W. Shi, G. Yang and P. Cheng, Rapid Detection of the Biomarkers for Carcinoid Tumors by a Water Stable Luminescent Lanthanide Metal-Organic Framework Sensor, *Adv. Funct. Mater.*, 2018, **28**, 1707169.

56 L. Wang, G. Fan, X. Xu, D. Chen, L. Wang, W. Shi and P. Cheng, Detection of polychlorinated benzenes (persistent organic pollutants) by a luminescent sensor based on a lanthanide metal-organic framework, *J. Mater. Chem. A*, 2017, **5**, 5541.

57 G. M. Sheldrick, A short history of SHELX, *Acta Crystallogr., Sect. A: Found. Crystallogr.*, 2008, **64**, 112.

58 G. M. Sheldrick, Crystal structure refinement with SHELXL, *Acta Crystallogr., Sect. C: Struct. Chem.*, 2015, **71**, 3.

59 S. P. Cook and G. H. Dieke, 6P state of the Gd^{+++} ion, *J. Chem. Phys.*, 1957, **27**, 1213.

60 G. H. Dielre and L. Leopold, Absorption, fluorescence, and magnetic properties of gadolinium chloride ($GdCl_3{\cdot}6H_2O$), *J. Opt. Soc. Am.*, 1957, **47**, 944.

61 M. Latva, H. Takalo, V. M. Mukkala, C. Matachescu, J. C. Rodríguez-Ubis and J. Kankare, Correlation between the lowest triplet state energy level of the ligand and lanthanide(III) luminescence quantum yield, *J. Lumin.*, 1997, **75**, 149.

62 J. R. Lakowicz and G. Weber, Quenching of fluorescence by oxygen. Probe for structural fluctuations in macromolecules, *Biochemistry*, 1973, **12**, 4161.

63 N. Chadborn, J. Bryant, A. J. Bain and P. O'Shea, Ligand-Dependent Conformational Equilibria of Serum Albumin Revealed by Tryptophan Fluorescence Quenching, *Biophys. J.*, 1999, **76**, 2198.

64 F. Kokal and T. Azuml, Excitation Energy Dependence of the Phosphorescence to Fluorescence Quantum Yield Ratio of $NaNO_2$ Crystal. An Interplay between the Energy-Dependent Intersystem Crossing and Vibrational Relaxation, *J. Phys. Chem.*, 1982, **86**, 177.

65 R. M. Hochstrasser and A. P. Marchetti, Electronic, Vibrational, and Zeeman Spectra of Triplet NO_2^-, *J. Chem. Phys.*, 1969, **50**, 1727.

66 S. Hinojosa, M. A. Meneses-Nava, O. Barbosa-Garcıa, L. A. Dıaz-Torres, M. A. Santoyo and J. F. Mosino, Energy back transfer, migration and energy transfer (Yb-to-Er and Er-to-Yb) processes in Yb, Er:YAG, *J. Lumin.*, 2003, **102103**, 694.